



Spatial and Temporal Pattern Changes and Driving Forces: Analysis of Salinization in the Yellow River Delta from 2015 to 2020

Authors: Mengmeng, Hong, Juanle, Wang, and Baomin, Han

Source: Journal of Resources and Ecology, 13(5) : 786-796

Published By: Institute of Geographic Sciences and Natural Resources Research, Chinese Academy of Sciences

URL: <https://doi.org/10.5814/j.issn.1674-764x.2022.05.004>

BioOne Complete (complete.BioOne.org) is a full-text database of 200 subscribed and open-access titles in the biological, ecological, and environmental sciences published by nonprofit societies, associations, museums, institutions, and presses.

Your use of this PDF, the BioOne Complete website, and all posted and associated content indicates your acceptance of BioOne's Terms of Use, available at www.bioone.org/terms-of-use.

Usage of BioOne Complete content is strictly limited to personal, educational, and non - commercial use. Commercial inquiries or rights and permissions requests should be directed to the individual publisher as copyright holder.

BioOne sees sustainable scholarly publishing as an inherently collaborative enterprise connecting authors, nonprofit publishers, academic institutions, research libraries, and research funders in the common goal of maximizing access to critical research.

J. Resour. Ecol. 2022 13(5): 786-796
DOI: 10.5814/j.issn.1674-764x.2022.05.004
www.jorae.cn

Spatial and Temporal Pattern Changes and Driving Forces: Analysis of Salinization in the Yellow River Delta from 2015 to 2020

HONG Mengmeng^{1,2}, WANG Juanle^{2,*}, HAN Baomin¹

1. School of Civil and Architectural Engineering, Shandong University of Technology, Zibo, Shandong 255049, China;
2. State Key Laboratory of Resources and Environmental Information System, Institute of Geographic Sciences and Natural Resources Research, Chinese Academy of Sciences, Beijing 100101, China

Abstract: China's Yellow River Delta represents a typical area with moist semi-humid soil salinization, and its salinization has seriously affected the sustainable use of local resources. The use of remote sensing technology to understand changes in the spatial and temporal patterns of salinization is key to combating regional land degradation. In this study, a feature space model was constructed for remote sensing and monitoring land salinization using Landsat 8 OLI multi-spectral images. The feature parameters were paired to construct a feature space model; a total of eight feature space models were obtained. An accuracy analysis was conducted by combining salt-loving vegetation data with measured data, and the model demonstrating the highest accuracy was selected to develop salinization inversion maps for 2015 and 2020. The results showed that: (1) The total salinization area of the Yellow River Delta displayed a slight upward trend, increasing from 4244 km² in 2015 to 4629 km² in 2020. However, the area's salting degree reduced substantially, and the areas of saline soil and severe salinization were reduced in size; (2) The areas with reduced salinization severity were mainly concentrated in areas surrounding cities, and primarily comprised wetlands and some regions around the Bohai Sea; (3) Numerous factors such as the implementation of the "Bohai Granary" cultivation engagement plan, increase in human activities to greening local residential living environments, and seawater intrusion caused by the reduction of sediment contents have impacted the distribution of salinization areas in the Yellow River Delta; (4) The characteristic space method of salinization monitoring has better applicability and can be promoted in humid-sub humid regions.

Key words: salinization; land degradation; feature space; salt-loving vegetation; the Yellow River Delta

1 Introduction

Land degradation poses a serious threat to terrestrial ecosystems. In the "Transforming our World: The 2030 Agenda for Sustainable Development" promulgated by the United Nations in 2016 (Guo, 2018), the SDG 15.3.1 goal is to halt the expansion of areas impacted by land degradation. Soil salinization, a form of land degradation, is caused by a rise in groundwater levels and surface water evaporation (Niu,

2016). Soil salinization typically occurs in areas where the groundwater level is high and the water contains high levels of soluble salts. The areas impacted by soil salinization in China are estimated to have expanded up to 3.6×10^5 km² and are primarily concentrated in Xinjiang, Gansu, and the Yellow River Delta (Bian et al., 2020). The Yellow River Delta represents a typical humid-semi-humid salinization area with a high groundwater level and has serious problems

Received: 2021-10-10 **Accepted:** 2022-04-11

Foundation: The Strategic Priority Research Program of Chinese Academy of Sciences (XDA19040501); The Construction Project of the China Knowledge Center for Engineering Sciences and Technology (CKCEST-2021-2-18).

First author: HONG Mengmeng, E-mail: hongmm@lreis.ac.cn

***Corresponding author:** WANG Juanle, E-mail: wangjl@igsnr.ac.cn

Citation: HONG Mengmeng, WANG Juanle, HAN Baomin. 2022. Spatial and Temporal Pattern Changes and Driving Forces: Analysis of Salinization in the Yellow River Delta from 2015 to 2020. *Journal of Resources and Ecology*, 13(5): 786-796.

associated with mineralization and salinization. In recent years, seawater intrusion has exacerbated the problems caused by salinization in the Yellow River Delta to the point of severely restricting the development of local agriculture (Zhou et al., 2017; Ke et al., 2021; Zhang et al., 2021).

Recently, domestic and foreign scholars have conducted extensive research on the use of imaging to remotely sense and monitor soil salinization changes via two major approaches. One includes determining the degree of salinization through semi-automatic methods such as supervised classification, while the other involves monitoring salinization by the construction of an inversion model. The former approach combines the threshold values of the Normalized Difference Vegetation Index (NDVI) and Salinity Index (SI). Xv et al. (2003) combined the NDVI and supervision classification to monitor the distribution of soil salinization in the Qingtongxia Irrigation Area. He et al. (2006) used the decision tree classification method to set each node classifier, and the results validated the extraction of information on saline land in Xinjiang. Huang et al. (2021) used the gray-level co-occurrence matrix method to extract second-order moment, contrast, entropy, correlation, and other texture feature information of remote sensing images. This information was then combined with NDVI, SI, and other spectral feature information through pre-set classification rules to realize the salt contents of the Yellow River Delta Kenli District's soil. Feng et al. (2019) used the method of combining supervision classification and visual interpretation to extract salinization information from Xinjiang Weiku Oasis. Furthermore, Han (2018) used supervised classification combined with decision tree methods to systematically study the dynamic change process of soil salinization in the Manas River Basin in the past 27 years. Unfortunately, the semi-automatic method combined with supervised classification cannot fully realize the automatic detection of salinization. Errors in supervised classification can interfere with the image classification accuracy in the verification result.

In the second method of monitoring salinization, that is, by the construction of an inversion model, the representative model is the back-propagation (BP) neural network model. Fan et al. (2015) previously compared the BP neural network inversion model with a mathematical statistics model, showing that the accuracy of the BP neural network model is superior to that of the traditional multiple regression model. Moreover, the inversion model is more suitable for the inversion mapping of soil salinization in high-salinity areas and has strong prospects for practical applications (Zhang et al., 2013). However, the BP network neural model is complicated to operate and has specific requirements for remote sensing images. Furthermore, this model cannot be applied in a wide range of applications. Lu et al. (2011) an-

alyzed the driving force of soil salinization in the Weigan River Basin of Xinjiang. The research showed that soil salinization is a combination of natural factors and human factors. Natural factors are the soil-formation conditions. Human factors are caused by human activities. Yao et al. (2015) analyzed the driving forces of oasis salinization in the arid areas of northwest China. His research showed that over the past 50 years, the main driving forces of oasis salinization in Yutian were human factors.

The feature space method is considered to be a simple, desirable, and effective remote sensing automatic detection method for salinization (Zhang, 2016). It is widely used for detecting the spatial distribution of salinization in arid and semi-arid areas. Dong et al. (2019) established a remote sensing monitoring model for soil salinization using data from Pan and Multispectral Sensor (PMS), Operational Land Imager (OLI), and Thematic Mapper (TM). They combined these data with the vegetation growth and SI to invert the salinization of Shouguang City. Based on the Landsat multispectral image, Rocha et al. (2017) used the principal component analysis method to prove that the two bands of SWIR-1 and SWIR-2 are more sensitive to the detection of soil salinization. Feng et al. (2018) proposed the Albedo-MSAVI feature space concept based on the Landsat 8 OLI multispectral image and built the salinization vegetation monitoring index (SDI) model. Du et al. (2018) proposed an improved salinization index (MSI) in the pomegranate-Dunhuang region of Gansu Province. They applied it to the model construction of feature space and got the improved MSDI model. Lu et al. (2020) applied improved soil to regulate minimum Soil Adjusted Vegetation Index (MSAVI) in Hetao irrigation area of Inner Mongolia. They built an improved salinization Monitoring Index (MSDI) model based on MSAVI, which is more accurate. Bian et al. (2020) used the Kenli District of Dongying City as a research area to propose a high-precision SI-albedo model based on Landsat images.

In recent years, the central government has carried out extensive work to solve the problems existing in the Yellow River basin. It has built the “four beams and eight pillars”^① for the protection and treatment of the Yellow River, rectified ecological and environmental problems, promoted ecological protection and restoration, improved the governance system, and made new progress in high-quality development. The policy of “Bohai Granary”^② was promoted to improve local salinization problems in the Yellow River Delta region. The Yellow River Delta is a typical humid sub humid area with serious salinization issues. The applicability of the two-dimensional (2D) feature space in this area is still lacking

① The “four beams and eight pillars” theory is a reform thinking and methodology put forward by the CPC Central Committee of China.

② “Bohai Granary” is an agricultural science and technology demonstration project to meet the major demand of national food security and to solve the problem that salinized land around Bohai Sea restricts food production.

in systematic exploration. Existing feature space explorations of humid sub humid regions are restricted to local regions and specific periods and cannot be broadly applied. Against the backdrop of these challenges, the Yellow River Delta region has been used to model the linear and nonlinear feature space. The related linear or nonlinear features are constructed according to the data distribution state of each characteristic parameter. These models were combined with measured data, including the salt-loving vegetation map, to determine the most accurate feature space model. This study serves as a preliminary exploration of the feature space method's applicability in determining the spatial distribution of salinization in humid sub humid regions.

2 Materials

2.1 Study area

The Yellow River Delta is located in the northeast part of Dongying City, Shandong Province, close to the Bohai Sea. The region is an alluvial plain that has been formed by the deposition of sediment in the Bohai Depression at the mouth of the Yellow River. The research area for this study comprised of the modern Yellow River Delta, including Kenli

District, Hekou District, Gudao Town, and other areas in Dongying City between 118°08'02"E–119°18'02"E, 37°21'26"N–38°09'14"N. This region has four distinct seasons with cool winters and hot summers. The salinization of the Yellow River Delta is relatively severe and is affected by the anti-salt phenomenon of groundwater which is not conducive for the growth of vegetation. The main halophytes that grow in this region are *Tamarix*, *Suaeda*, and *Phragmites australis*.

2.2 Data sources and pre-processing

Landsat 8 OLI multispectral remote sensing images with a spatial resolution of 30 m were selected as a data source. The remote sensing images dated April 15, 2015, and April 23, 2020 were selected for feature space inversion of salinization due to the lack of vegetation growth in the Yellow River Delta in April. Surface salinity increases in spring. The salt from underground rises to the surface, forming a salt crust on top of the soil. This increases the surface reflectivity. ENVI5.3 software was used to pre-process the selected remote sensing images, including image radiometric calibration (Radiometric calibration) and atmospheric correction (FLASSH atmospheric correction).

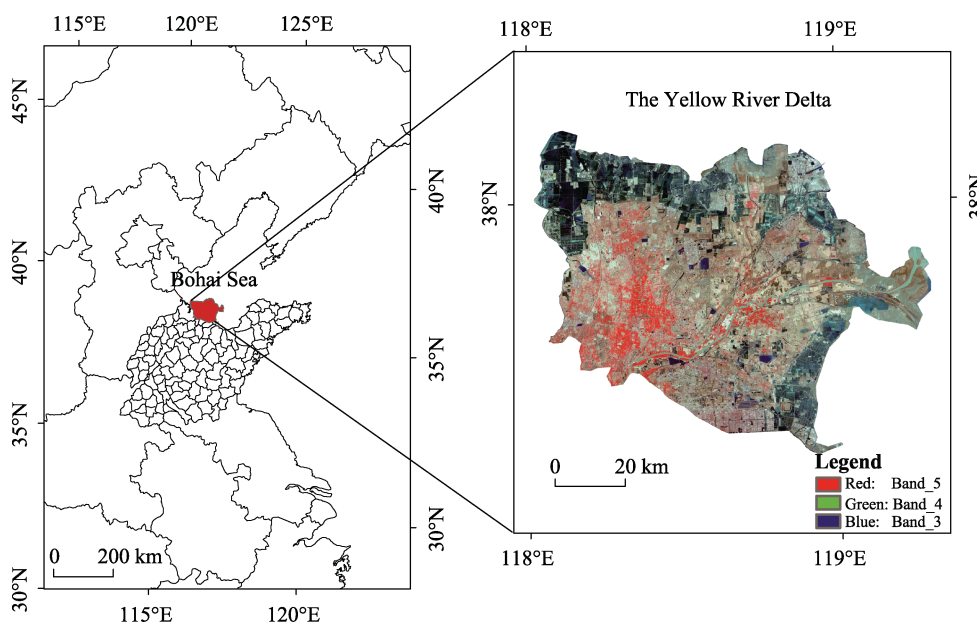


Fig. 1 Study area

The field observation data used for accuracy verification included data measured from 36 sample points in 2015 and 40 sample points in 2020. The sample point data included longitude, latitude, electrical conductivity (EC), salt content, and pH. The latitude and longitude of the sample points were measured by GPS-RTK in real-time, and the positioning was accurate to the centimeter level. The EC, salt content, pH value, and other indices of the sample points were measured and analyzed by the professional soil analysis laboratory of Yucheng Station of the Chinese Academy of Sciences.

3 Method

3.1 Principles of feature space

According to the characteristics of each index paired combination, this experiment can be divided into two categories: linear feature space and nonlinear feature space. The following examples illustrate the principles of the linear feature space and nonlinear feature space.

3.1.1 Linear feature space

Studies have shown that the surface albedo and salinity index are positively correlated with the degree of salinization.

Albedo is positively correlated with the salinity index (Fig. 2a). A represents the point with the highest surface albedo and the lowest salt index, B represents the point with the lowest surface albedo and the lowest salt index, C represents the point with the lowest surface albedo and the highest salt index, and D represents the point with the highest surface albedo and the highest salt index. All salinization grades are included within the ABCD range and show different distributions depending on the selected model. Based on this, a model could be used to invert the salinization distribution and establish a linear feature space.

3.1.2 Nonlinear feature space

Relevant studies have demonstrated a significant positive correlation between the salinity index and salinization degree. Due to the growth of salt-loving vegetation, the Vegetation Coverage Index value and the degree of salinization show a non-linear relationship. As shown in Fig. 2b, A represents the highest salinity index which occurred with a moderate vegetation index; B represents the lowest point of the salinity index and the lowest point of vegetation coverage; C represents the lowest point of the salinity index and the highest point of vegetation coverage. All salinization grades were covered within the ABC range and displayed different distributions according to the selected model. Based on this, a nonlinear space could be constructed.

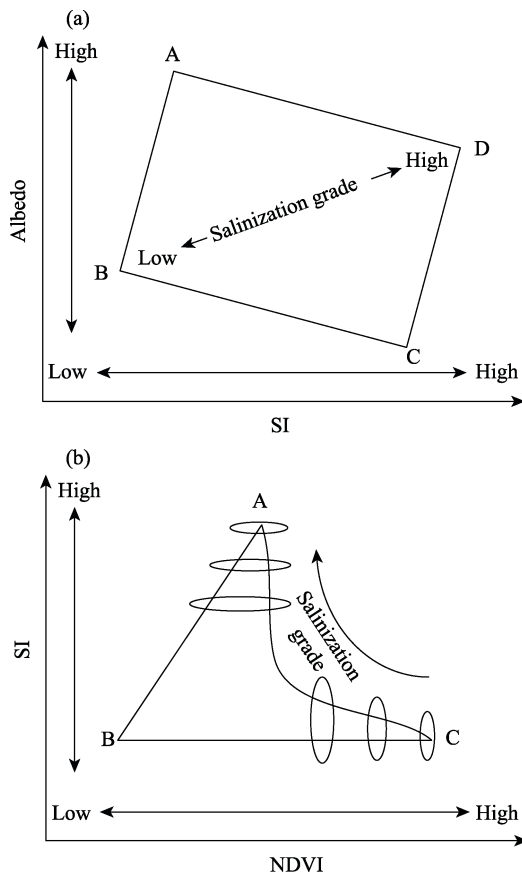


Fig. 2 Principle of linear feature space (a) and nonlinear feature space (b)

3.2 Selection of inversion parameters

In this study, the following indices were used for soil salinization: Surface albedo (Albedo), Normalized Vegetation Index (NDVI), Salinity Index (SI), and Minimum Soil Adjusted Vegetation Index (MSAVI).

3.2.1 Surface albedo

Albedo refers to the ability of objects on the earth’s surface to reflect solar radiation. The spectral characteristics are different, thus the Albedo index varies substantially. As the level of salinization changes, the texture of the ground changes, and the reflectivity of the ground surface varies. Therefore, Albedo is a useful indicator for measuring the level of salinization. Its formula is as follows:

$$Albedo = 0.356B + 0.13R + 0.373NIR + 0.085SR1 + 0.072SR2 - 0.0018 \tag{1}$$

where B, R, NIR, SR1, and SR2 correspond to the reflectance values of Landsat 8 OLI’s multispectral images in blue, red, near-infrared, short-infrared 1, and short-infrared 2 bands, respectively.

3.2.2 Salt Index and Derivative Index

The SI reflects the spectral reflectivity of the salt crust on the soil surface. The SI plays an important role in measuring the degree of soil salinization. SI1 attempts to integrate the green band into the salt index to explore its effect on salinization, while SI2 aims to use different band combination formula to explore the sensitivity of different combination formula to salinization. The formula is as follows:

$$SI = \sqrt{B \times R} \tag{2}$$

where B and R correspond to the reflectance values of Landsat 8 OLI’s multispectral images in blue and red bands, respectively.

$$SI1 = \sqrt{G \times R} \tag{3}$$

where G and R correspond to the reflectance values of Landsat 8 OLI’s multispectral images in green and red bands, respectively.

$$SI2 = \sqrt{G^2 + R^2} \tag{4}$$

where G and R correspond to the reflectance values of Landsat 8 OLI’s multispectral images in green and red bands, respectively.

3.2.3 Normalized Vegetation Index

NDVI, another useful indicator for measuring soil salinization, reflects vegetation coverage. Different levels of salinization and different vegetation on the ground cause deviations in the NDVI values. Its formula is as follows:

$$NDVI = (NIR - R) / (NIR + R) \tag{5}$$

where NIR and R correspond to the reflectance values of Landsat 8 OLI’s multispectral images in near-infrared and red bands, respectively.

3.2.4 Soil Adjustment Vegetation Index

MSAVI is a kind of vegetation index. Compared with other vegetation indexes, MSAVI eliminates the impact of bare

soil on vegetation and can more accurately reflect the vegetation coverage in salinized areas. The formula is as follows:

$$MSAVI = (2NIR + 1 - \sqrt{(2NIR + 1)^2 + 8(NIR - R)}) / 2 \quad (6)$$

where NIR and R correspond to the reflectance values of Landsat 8 OLI's multispectral images in near-infrared and red bands, respectively.

3.3 Parameter normalization

To calculate the normalized index, the maximum and minimum values of $Albedo$, $NDVI$, $MSAVI$, SI , $SI1$, and $SI2$ were calculated, and each value was entered into the following formula:

$$A = \frac{Albedo - Albedo_{min}}{Albedo_{max} - Albedo_{min}} \times 100\% \quad (7)$$

where A represents the normalized $Albedo$ value, $Albedo_{min}$ represents the minimum value of $Albedo$, and $Albedo_{max}$ represents the maximum value of $Albedo$.

$$N = \frac{NDVI - NDVI_{min}}{NDVI_{max} - NDVI_{min}} \times 100\% \quad (8)$$

where N represents the normalized $NDVI$ value, $NDVI_{min}$ represents the minimum value of $NDVI$, and $NDVI_{max}$ represents the maximum value of $NDVI$.

$$M = \frac{MSAVI - MSAVI_{min}}{MSAVI_{max} - MSAVI_{min}} \times 100\% \quad (9)$$

where M represents the normalized $MSAVI$ value, $MSAVI_{min}$ represents the minimum value of $MSAVI$, and $MSAVI_{max}$ represents the maximum value of $MSAVI$.

$$S = \frac{SI - SI_{min}}{SI_{max} - SI_{min}} \times 100\% \quad (10)$$

where S represents the normalized SI value, SI_{min} represents the minimum value of SI , and SI_{max} represents the maximum value of SI .

$$SI1 = \frac{SI1 - SI1_{min}}{SI1_{max} - SI1_{min}} \times 100\% \quad (11)$$

where $SI1$ represents the normalized $SI1$ value, $SI1_{min}$ represents the minimum value of $SI1$, and $SI1_{max}$ represents the maximum value of $SI1$.

$$SI2 = \frac{SI2 - SI2_{min}}{SI2_{max} - SI2_{min}} \times 100\% \quad (12)$$

where $SI2$ represents the normalized $SI2$ value, $SI2_{min}$ represents the minimum value of $SI2$, and $SI2_{max}$ represents the maximum value of $SI2$.

4 Results and analysis

4.1 Building the feature space

To obtain a specific inversion model of the feature space, a total of 520 uniformly distributed points from the study area were selected. The $Albedo$, $NDVI$, $MSAVI$, SI , $SI1$, and $SI2$ index were extracted from the pixel where each point was located.

4.1.1 Linear model construction

SPSS software was used for statistical analysis, and the linear relationship between the relevant feature vectors was obtained. Through learning the linear classification model of desertification, the linear classification model of salinization was obtained, and its formula is as follows:

$$SS = K \times X_1 - X_2 \quad (13)$$

where SS refers to the salinization level, K is the negative reciprocal of the fitted straight line in the feature space, X_1 is one of the feature indices, and X_2 is the remaining related feature indices excluding X_1 . Four linear feature spaces are constructed, as shown in Fig. 3.

As shown in Fig. 3a, the $Albedo$ - SI model is referred to as AS , where K is the negative derivative of slope, X_1 is $Albedo$, X_2 is SI . Its formula is as follows:

$$AS = -1.54 \times Albedo - SI \quad (14)$$

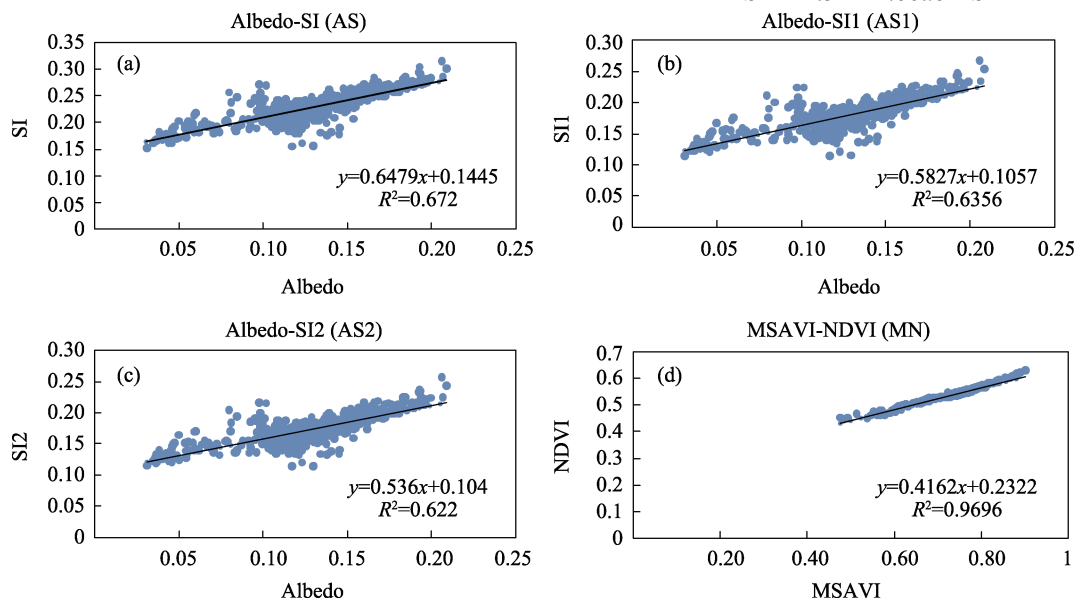


Fig. 3 Linear space AS (a), AS1 (b), AS2 (c) and MN (d).

As shown in Fig. 3b, the Albedo-SI1 model is referred to as *AS1*, where *K* is the negative derivative of slope, X_1 is *Albedo*, X_2 is *SI1*. Its formula is as follows:

$$AS1 = -1.76 \times Albedo - SI1 \quad (15)$$

As shown in Fig. 3c, the Albedo-SI2 model is referred to as *AS2*, where *K* is the negative derivative of slope in the figure, X_1 is *Albedo*, X_2 is *SI2*. Its formula is as follows:

$$AS2 = -1.86 \times Albedo - SI2 \quad (16)$$

As shown in Fig. 3d, the MSAVI-NDVI model is referred to as *MN*, where *K* is the negative derivative of slope in the figure, X_1 is *MSAVI*, X_2 is *NDVI*. Its formula is as follows:

$$MN = -2.4 \times MSAVI - NDVI \quad (17)$$

4.1.2 Non-linear model construction

The extraction results of each index were imported into ENVI 5.3, and a 2D scatter plot was used to obtain the distribution characteristics of the correlation relationship between the feature vectors of each pixel in the study area.

In the Albedo-NDVI feature space model, a 2D scatter plot was created with the vegetation coverage shown on the x-axis and the surface albedo plotted on the y-axis. As shown in Fig.4a, the surface albedo and vegetation coverage exhibited a significant non-linear relationship. The point (0, 1) in the *NDVI* and *Albedo* coordinate system was used as a reference point. Points most proximate to this reference

point possess the highest salinization levels. On this basis, the NDVI-Albedo nonlinear model was constructed and named NANM (NDVI-Albedo nonlinear model). Its formula is as follows:

$$NANM = \sqrt{NDVI^2 + (Albedo - 1)^2} \quad (18)$$

As shown in Fig. 4b, in the MANM feature space model, *Albedo* and *MSAVI* show a significant nonlinear relationship. The point (0.7, 0.5) in *MSAVI* and *Albedo* coordinate system was taken as the reference point. The closer the distance to the reference point, the higher the salinization level was. On this basis, the MSAVI-Albedo nonlinear model is constructed and named MANM (MSAVI-Albedo nonlinear model), and its formula is as follows:

$$MANM = \sqrt{(MSAVI - 0.7)^2 + (Albedo - 0.5)^2} \quad (19)$$

As shown in Fig. 4c, in the NSNM characteristic space model, *NDVI* and *SI* present a significant nonlinear relationship. The point (1, 0) in the *NDVI* and *SI* coordinate system is taken as the reference point. The closer the distance to the reference point, the higher the salinization grade is. Named as NSNM (NDVI-SI nonlinear Model), and its formula is as follows:

$$NSNM = \sqrt{(NDVI - 1)^2 + SI^2} \quad (20)$$

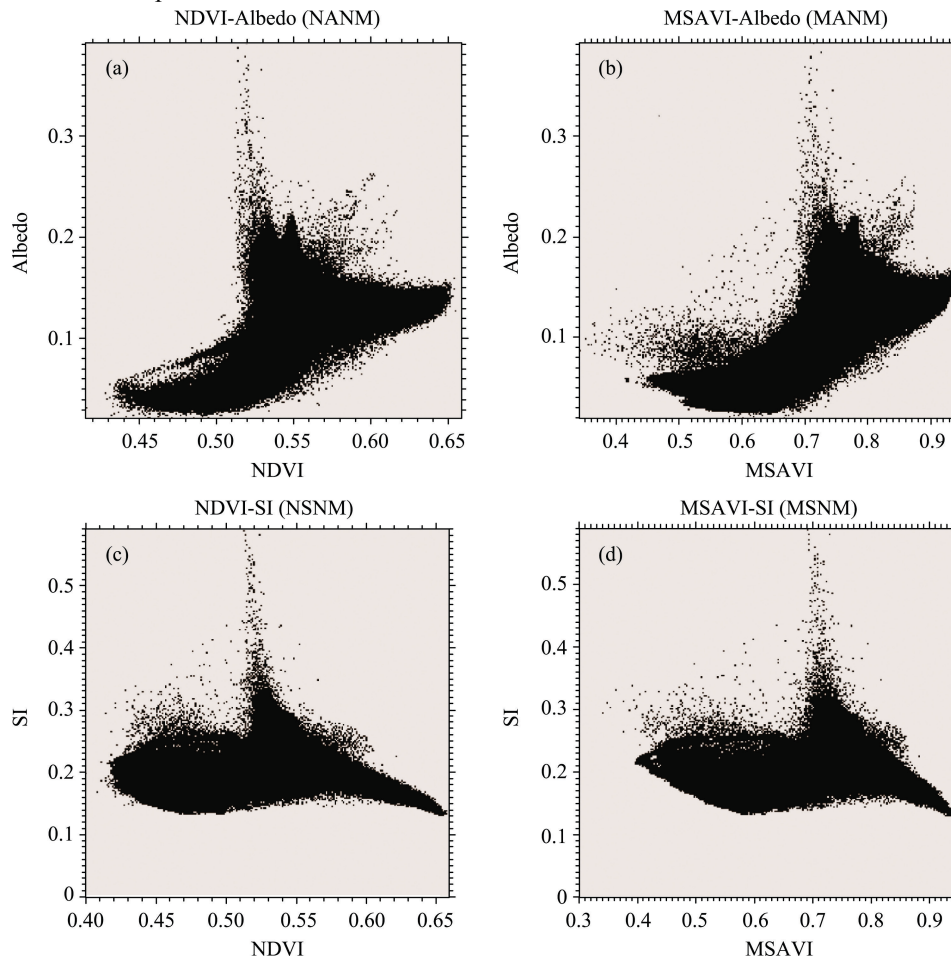


Fig. 4 Non-linear space NANM (a), MANM (b), NSNM (c) and MSNM (d).

As shown in Fig. 4d, in the MSNM characteristic space model, there is a significant nonlinear relationship between *MSAVI* and *SI*. The point (1, 1) in the *MSAVI* and *SI* coordinate systems is taken as the reference point. The closer the distance to the reference point, the higher the salinization level. On this basis, the *MSAVI-SI* nonlinear model is constructed and named *MSNM* (*MSAVI-SI* Nonlinear Model), and its formula is as follows:

$$MSNM = \sqrt{(MSAVI - 1)^2 + (SI - 1)^2} \quad (21)$$

4.2 Inversion distribution of salinity

The linear and nonlinear models were used for image inversion to obtain the salinization inversion map of the Yellow River Delta area. The Jenk Natural Break Point classification method was used. This classification method is divided into five categories: saline soil, severe salinization, moder-

ate salinization, mild salinization, and non-salinization. The classification intervals are as follows:

Based on the most accurate NSNM feature space model, an inversion map of the lower Yellow River and adjacent coastal areas in 2020 was obtained, as shown in Fig. 5a. It has an accuracy of 67.5%. The 2020 inversion map revealed that the selected study area was dominated by moderate salinization. Mild salinization and non-salinized soils were mainly distributed near the Yellow River and the southwestern region. Severe salinization and saline soils were mainly distributed in the coastal areas. In 2020, 76.25% of the total study area was salinized. Within the salinized areas, 2874 km² (47.36%) was moderately salinized, 764 km² (12.58%) was lightly salinized, 673 km² (11.09%) was heavily salinized, and 317 km² (5.22%) of the total area was comprised of saline soil.

Table 1 Classification of salinization grades

Degree of salinization	Non salinization	Mild salinization	Moderate salinization	Severe salinization	Saline soil
<i>AS</i>	≤ 0.56	$0.56 < AS \leq 0.65$	$0.65 < AS \leq 0.74$	$0.74 < AS \leq 0.83$	> 0.83
<i>AS1</i>	≤ 0.59	$0.59 < AS1 \leq 0.67$	$0.67 < AS1 \leq 0.74$	$0.74 < AS1 \leq 0.80$	> 0.80
<i>AS2</i>	≤ 0.59	$0.59 < AS2 \leq 0.66$	$0.66 < AS2 \leq 0.73$	$0.73 < AS2 \leq 0.80$	> 0.80
<i>MN</i>	≤ 0.1	$0.1 < MN \leq 0.17$	$0.17 < MN \leq 0.24$	$0.24 < MN \leq 0.31$	> 0.31
<i>NANM</i>	≤ 0.85	$0.85 < NANM \leq 0.89$	$0.89 < NANM \leq 0.94$	$0.94 < NANM \leq 0.97$	> 0.97
<i>MANM</i>	≤ 0.60	$0.60 < MANM \leq 0.68$	$0.68 < MANM \leq 0.74$	$0.74 < MANM \leq 0.78$	> 0.78
<i>NSNM</i>	≤ 0.84	$0.84 < NSNM \leq 0.88$	$0.88 < NSNM \leq 0.89$	$0.89 < NSNM \leq 0.91$	> 0.91
<i>MSNM</i>	≤ 0.79	$0.79 < MSNM \leq 0.83$	$0.83 < MSNM \leq 0.86$	$0.86 < MSNM \leq 0.89$	> 0.89

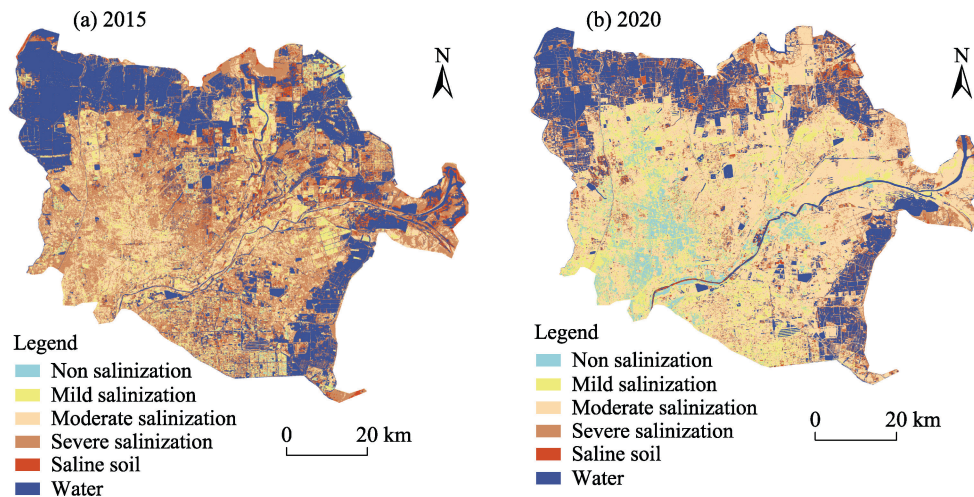


Fig. 5 Distribution of salinization in 2015 (a) and 2020 (b)

The spatial distribution of salinization in the lower Yellow River and adjacent coastal areas in 2015 was determined using the same method and is shown in Fig. 5b. It has an accuracy of 75%. As shown in the Fig. 5b, the study area was dominated by severe salinization in 2015. Saline soil and severe salinization areas were mainly distributed in the northeastern portions of the study area. Moderate and mild

salinization areas were mainly distributed near the Yellow River and southwestern region; non-salinization areas were scattered around the Yellow River. In 2015, 70% of the total study area was salinized. Within the salinized areas, 2088 km² (34.4%) was heavily salinized, 1295 km² (21.3%) was moderately salinized, 403 km² (6.7%) was lightly salinized, and 456 km² (7.6%) of the total area was comprised of sa-

line soil.

A comparison of data between the years 2015 to 2020 revealed that saline soil decreased by 2.38%, and heavily salinized areas decreased by 23.31%. This implies that the salinization level decreased in the study area. It was also noted that moderate salinization areas increased by 26.06%, and lightly salinized areas increased by 4.39%. This was because some saline soil areas and heavily salinization areas became moderate or lightly salinized areas. Thus, it shows that the degree of salinization has generally decreased.

4.3 Accuracy verification

According to China's soil salinization grading standards and Lu Rukun's 2000 "Soil Agricultural Chemistry Analysis and Methods" (Lu, 2000), the degree of soil salinization in humid sub humid, arid-semi-arid areas is divided into the following five categories: non-saline soil (soil salinity <1.0); mildly salinized soil ($1.0 \leq \text{soil salinity} < 2.0$); moderately salinized soil ($2.0 \leq \text{soil salinity} < 4.0$); severe saline soil ($4.0 \leq \text{soil salinity} < 6.0$); saline soil (soil salinity >6.0). The field measurement sample data were salinized and classified according to these standards. A quantitative analysis was performed using the feature space model inversion to determine the salinization degree of measurement point locations.

Table 2 Accuracy analysis of each model

Model	Correct classification	Misclassification	Accuracy (%)
AS	17	23	42.5
AS1	15	25	37.5
AS2	17	23	42.5
MN	23	17	57.5
NANM	16	24	40
MANM	20	20	50
NSNM	27	13	67.5
MSNM	19	21	47.5

Based on these data, the 2020 NSNM nonlinear feature space model demonstrated a higher accuracy of 67.5%. The 2015 data were also tested following this method; the Albedo-SI model demonstrated the strongest applicability to the 2015 data, with an accuracy of 75%. The Jenk Natural Break Point classification method was adopted after remote sensing image inversion. However, in the study of salinization, the Jenk Natural Break Point classification method has certain instability, which leads to a decrease in accuracy. The accuracy of the classification results is however more reliable in comparison with similar products. This study has been compared with the distribution halophilic plants. The results show that the spatial distribution of the classification results is reasonable in this region. The results of quantitative inversion show that the overall decrease of salinization is consistent with reality. These spatiotemporal perceptions

can provide data and methodological support for land degradation control and sustainable development in this region.

5 Discussion

5.1 Applicability of the feature space method

In comparison to the semi-automated remote sensing monitoring method combined with supervised classification and the more complex neural network method, the 2D feature space method is a simpler, more desirable, and more effective remote automatic detection method for salinization (Zhang, 2016). The main problem is the effective application of remote detection technology in geoscience. The construction of a simple, fast, effective, and widely applicable soil salinization monitoring method has become a major challenge. Compared with the more complex network neural models in the existing research pools and the semi-automatic detection methods that require part of the labor, the 2D feature space method can be considered advantageous because of its simplicity, convenience, and complete automation.

This study uses salt-loving vegetation to analyze the applicability of the feature space method. As shown in Fig. 4, when compared with the map of salt-loving vegetation near the lower Yellow River in 2015, the areas of arable land in the north-eastern part of the Yellow River Delta had expanded while the areas of salt-loving vegetation had shrunk by 2020. From this information, combined with analysis of the spatial salinization distribution map in 2015 and 2020, it can be seen that: 1) The overall salinization area within the study area is on the rise; expanded areas were primarily comprised of areas with wetlands and coastal bodies of water. 2) Most of the salinization reduction areas are distributed in urban areas and areas with increased rice cultivation, such as Gudao Town, Hekou District, Dongying City, Kenli District, and Zhengda Science and Technology Ecological Park. The salinization area aggravates mostly for wetlands and parts of coastal areas.

5.2 Analysis of the causes of reduced salinization

The causal agents of salinization changes in the Yellow River Delta can be divided into the following three categories: 1) Improvements in the activities of residents. The improvement of residential areas, such as in the cases of planting crops like cotton and apple trees on a small-scale, adopting cow manure composting in crop rotations, and completing greening renovations in urban areas can have positive effects on remediating local salinization (Xiao, 2018; Liu et al., 2020). 2) Since undertaking the "Bohai Granary" technology demonstration project, Dongying City has established and perfected saline-alkali land development processes as well as medium- and low-yield field transformation technology systems, which focus on altering salt levels and increasing the volume of agricultural land. Based on official government records, Dongying City has essentially matched the output level of medium-yield fields by

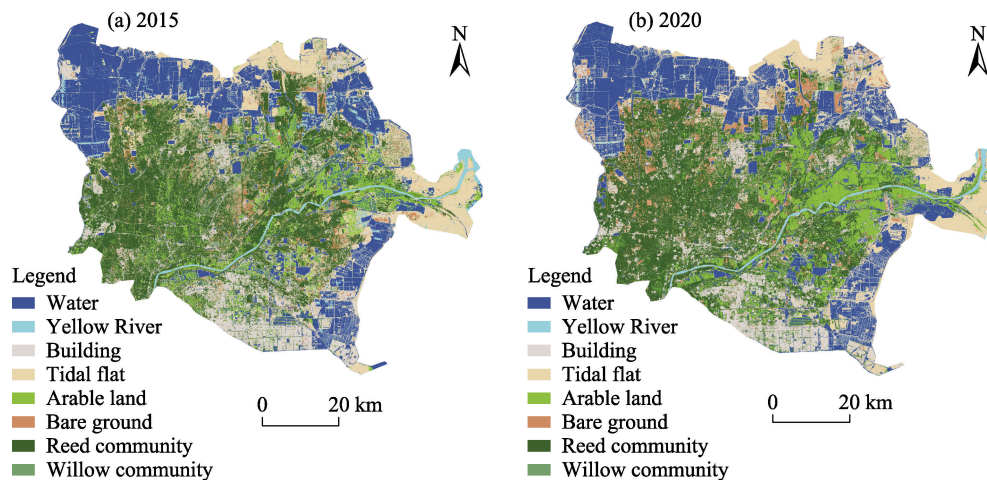


Fig. 6 Distribution map of salt-loving vegetation in 2015 (a) and 2020 (b)

transforming 80 km² of alkali wasteland. Furthermore, the city has transformed approximately 200 km² of medium- and low-yield fields into medium- and high-yield fields. This has effectively increased the overall yield of the city's existing rice planting area (Ma et al., 2020). Rice is often used for improving saline-alkali land. As a crop with moderate sensitivity to salt, it increases land-use efficiency. Planting rice in saline-alkali land causes the soil's surface salt to sink via irrigation. Moreover, paddy rotations following three years of continuous planting can lead to improved soil structure. Furthermore, the root systems of rice crops secrete organic acids which absorb salt from the soil environment. This, in effect, loosens the soil structure, which improves the soil's water storage capacity and aids in preventing secondary salinization (Leng et al., 2020). 3) In recent years, the water and sediment contents of the Yellow River have decreased. The water levels at the mouth of the Yellow River have decreased. However, the seawater level has remained high; this has led to seawater intrusion and an increase in salinized areas in the lower reaches of the Yellow River and other areas with high water content, such as wetlands and coastal areas (Chen and Fu, 2021).

5.3 Suggestions for salinization treatment

The results of this experiment support several recommendations for salinization prevention and treatment in the Yellow River Delta. 1) Continued execution of the "Bohai Granary" plan is recommended. The current rice acreage should be maintained with considerations for expansion. Rice cultivation can be extended to the mild salinization areas near the Yellow River basin and southwest of the study area. Human activities, including economic improvements, expansion of urban land, increased land reclamation rates, and other factors have positive corrective effects on reducing the volume of salinized land (Xiao, 2018). Therefore, it is recommended that activities such as the reclamation of small-scale farmland centered on human settlements and the positive transformation of the living environment are incentivized and

further promoted. 2) According to our analysis, seawater intrusion is a key driver in the expansion of salinized areas and a reduction of freshwater wetlands in the Yellow River Delta. The leading cause of seawater intrusion in the Yellow River Delta is the decrease in sand content; this ultimately destroys the sand filling and increases the area's seawater erosion rate. Accordingly, we recommend that the Yellow River Delta's sand contents be increased and that research and management efforts towards reversing seawater flow are prioritized. 3) Owing to developments derived from big data, additional data and platforms have become increasingly available such that rapid automatic data processing methods have become commonplace. Based on available data, utilizing the feature space model for remote sensing and monitoring salinization areas supports the implementation of a shared data platform to allow for swift automatic detection of salinization changes. This will enable further research on the method's efficacy and promote real-world geoscience applications.

6 Conclusions

To address the challenges posed by soil salinization monitoring in the Yellow River Delta, a feature space method was studied using Landsat 8 OLI imagery combined with field sampling salinity data. We studied the linear and non-linear relationships between seven indices. They are the Surface albedo, Soil Adjusted Vegetation Index (MSAVI), Salinity Index (SI), Salinity Index I (SI1), Salinity Index II (SI2), Vegetation Coverage Index (NDVI), and Soil Adjusted Vegetation Index (MSAVI). Through data analysis, a corresponding feature space model was constructed. The models demonstrating enhanced accuracy based on quantitative analysis and the salt-loving vegetation accuracy verification method were selected to obtain the salinization inversion maps for 2015 and 2020. The study's results revealed that although the overall land volume of salinized areas in the Yellow River Delta increased from 2015 to 2020, the mild salinization areas

expanded while the areas of severe and moderate salinization shrunk, and the total area's average salinization level showed a downward trend. A review of relevant literature indicates that the increase in areas impacted by salinization may be attributed to the effects of seawater intrusion, while the decrease in salinization level may be attributed to the planting of salt-tolerant plants such as rice or land transformation by residents. This study demonstrated the feature space model's efficacy in monitoring salinization areas. The data broadly supports future applications of this method to monitor other humid and semi-humid salinized areas.

References

- Bian L L, Wang J L, Guo B, et al. 2020. Remote sensing extraction of soil salinity in Yellow River Delta Kenli County based on feature space. *Remote Sensing Technology and Application*, 35(1): 211–218. (in Chinese)
- Chen Y P, Fu B J. 2021. The key issues of ecological protection and governance in different sections of the Yellow River Basin. Shanxi, China Science News. http://xab.cas.cn/tpxw/202103/t20210302_5967163.html.
- Dong F, Tang Y J, Xing X R, et al. 2019. Formation and evolution of soil salinization in Shouguang City based on PMS and OLI/TM sensors. *Water*, 11(2): 345. DOI: 10.3390/w11020345.
- Du T, Jiao J Z, Xie Y W, et al. 2018. Method exploration for quantitative evaluation of salinization using landsat satellite image: A case study of Guazhou-Dunhuang area. *Hubei Agricultural Sciences*, 57(1): 51–55. (in Chinese)
- Fan Y G, Li T T, Li X C. 2015. Soil salinization retrieval for the Yellow River Delta based on Landsat 8. *Shandong Agricultural Sciences*, 47(2): 119–124. (in Chinese)
- Feng J, Ding J L, Wei W Y. 2018. A study of soil salinization in Weigan and Kuqa Rivers Oasis based on Albedo-MSAVI feature space. *China Rural Water and Hydropower*, (2): 147–152. (in Chinese)
- Feng J, Ding J L, Wei W Y. 2019. Soil salinization monitoring based on radar data. *Remote Sensing for Land and Resources*, 31(1): 195–203. (in Chinese)
- Guo H D. 2018. A project on big earth data science engineering. *Bulletin of Chinese Academy of Sciences*, 33(8): 818–824. (in Chinese)
- Han Y. 2018. Dynamic monitoring and risk assessment of soil salinization in Manasi River Basin, Xinjiang. Diss., Shihezi, China: Shihezi University. (in Chinese)
- He Q S, Tashpolat T, Ding J L. 2006. The extraction of saline soil information in arid area based on decision tree algorithm: A case study in the delta oasis of Weigan and Kuqa rivers. *Resources Science*, 28(6): 134–140. (in Chinese)
- Huang J, Zhao G X, Xi X, et al. 2021. Extraction of soil salinization information by combining spectral and texture data in the Yellow River Delta: A case study in Kenli District, Shandong Province. *Journal of Agricultural Resources and Environment*, 38(3): 1–14. (in Chinese)
- Ke Z M, Liu X L, Ma L H, et al. 2021. Rainstorm events increase risk of soil salinization in a loess hilly region of China. *Agricultural Water Management*, 256: 107081. DOI: 10.1016/j.agwat.2021.107081.
- Leng C X, Zheng F Y, Zhao B P, et al. 2020. Advances on alkaline tolerance of rice. *Biotechnology Bulletin*, 36(11): 103–111. (in Chinese)
- Liu S L, Sun Z Q, Dong X X, et al. 2020. Effects of different crop rotation systems on soil chemical and physical characteristics and wheat yield in salinity croplands of the Yellow River Delta. *Shandong Agricultural Sciences*, 52(11): 60–64. (in Chinese)
- Lu J, Zhang X J, Ye P S, et al. 2020. Remote sensing monitoring of salinization in Hetao irrigation district based on SI-MSAVI feature space. *Remote Sensing for Land & Resources*, 32(1): 169–175. (in Chinese)
- Lu L, Qiao M, Zhou S B. 2011. Analysis on characteristics and driver forces of soil salinization in Weigan River Basin, Xinjiang. *Research of Agricultural Modernization*, 32(2): 357–361. (in Chinese)
- Lu R K. 2000. Soil argrochemistry analysis protocols. Beijing, China: China Agriculture Science Press. (in Chinese)
- Ma X M, Wu J Z, Xie Y M, et al. 2020. Implementation of science and technology demonstration project in Dongying City, Shandong Province. *World Tropical Agriculture Information*, (1): 10–11. (in Chinese)
- Niu Z Y, Ding J L, Li Y H, et al. 2016. Soil salinization information extraction method based on GF-1 image. *Arid Land Geography*, 39(1): 171–181. (in Chinese)
- Rocha N O, Teixeira A, Leão R, et al. 2017. Hyperspectral remote sensing for detecting soil salinization using ProSpecTIR-VS aerial imagery and sensor simulation. *Remote Sensing*, 9(1): 42. DOI: 10.3390/rs9010042.
- Xiao Y. 2018. Human activities and their effects on soil salinization and degradation in the Yellow River Delta. Diss., Shouguang, China: Shandong Agricultural University. (in Chinese)
- Xv D, Wang S L, Can L G, et al. 2003. Applied study on identification of crops and salinization distribution by NDVI Index. *Journal of Irrigation and Drainage*, 31(6): 5–8, 32. (in Chinese)
- Yao Y P, Wahap H, Fu J R. 2015. Analysis on the driving forces of oasis desertification and salinization in the arid region of Northwest China: A case study of Keriya Oasis. *Journal of Natural Science of Heilongjiang University*, 32(4): 519–525. (in Chinese)
- Zhang C W, Tang J K, Yu X J, et al. 2013. Quantitative retrieval of soil salt content based on remote sensing in the Yellow River Delta. *Journal of Graduate University of Chinese Academy of Sciences*, 30(2): 220–227. (in Chinese)
- Zhang W K. 2016. Remote sensing monitoring models of soil salinization in the Yellow River Delta based on featurespace. Diss., Qingdao, China: China University of Petroleum. (in Chinese)
- Zhang Z X, Song Y T, Zhang H Z, et al. 2021. Spatiotemporal dynamics of soil salinity in the Yellow River Delta under the impact of hydrology and climate. *Chinese Journal of Applied Ecology*, 32(4): 1393–1405. (in Chinese)
- Zhou M H, Butterbach-Bahl K, Vereecken H, et al. 2017. A meta-analysis of soil salinization effects on nitrogen pools, cycles and fluxes in coastal ecosystems. *Global Change Biology*, 23(3): 1338–1352.

黄河三角洲 2015–2020 盐渍化时空变化及成因分析

洪梦梦^{1,2}, 王卷乐², 韩保民¹

1. 山东理工大学建筑工程学院, 山东淄博 255049;

2. 中国科学院地理科学与资源研究所, 资源与环境信息系统国家重点实验室, 北京 100101

摘要:黄河三角洲是我国湿润-半湿润土壤盐渍化的典型地区, 其盐渍化现象已严重影响当地土壤资源的可持续利用。本研究利用 Landsat 8 OIL 多光谱影像, 运用 ENVI、ArcGIS 等软件提取研究区内的 7 个相关地表特征参量并将其两两组合, 构建特征空间模型, 选取其中拟合度较高的 8 个特征空间模型, 结合喜盐植被对其进行精度分析并筛选出精度最高的模型形成盐渍化反演图。结果表明: 2015 年 Albedo-SI 模型的适用性最高, 精度为 75%; 2020 年 NSNM 模型的适用性最高, 精度为 67.5%。研究结果显示: (1) 黄河三角洲盐渍化总体面积呈轻微上升趋势, 由 2015 年的 4244 km² 上升至 2020 年的 4629 km², 但其盐渍化程度显著下降, 盐土及重度盐渍化面积减少; (2) 盐渍化减轻地区主要分布在城市周边地区及水稻面积增多地区, 盐渍化加重地区为湿地及部分沿海地区; (3) “渤海粮仓”计划的实施、当地居民生活环境绿化改造等人类活动、黄河泥沙含量减少造成的海水倒灌等因素均对区域盐渍化分布造成影响; (4) 特征空间方法对盐渍化监测具有较好的适用性, 可以在更多湿润-半湿润地区推广。

关键词: 盐渍化; 土地退化; 特征空间; 喜盐植被; 黄河三角洲